Avalanches mediate crystallization in a hard-sphere glass

Avalanches mediate crystallization in a hard-sphere glass

Eduardo Sanz[a,b,1], Chantal Valeriani[a,b,1,2], Emanuela Zaccarelli[c], Wilson C. K. Poon[b], Michael E. Cates[b], and Peter N. Pusey[b]

[a]Departamento de Quimica Fisica I, Facultad de Ciencias Quimicas, Universidad Complutense de Madrid, 28040 Madrid, Spain; [b]Scottish Universities Physics Alliance, School of Physics and Astronomy, University of Edinburgh, Edinburgh EH9 3JZ, Scotland; and [c]Consiglio Nazionale delle Ricerche–Istituto dei Sistemi Complessi and Dipartimento di Fisica, Università di Roma La Sapienza, 00185 Rome, Italy

Edited by Frank H. Stillinger, Princeton University, Princeton, NJ, and approved November 7, 2013 (received for review May 3, 2013)

By molecular-dynamics simulations, we have studied the devitrification (or crystallization) of aged hard-sphere glasses. First, we find that the dynamics of the particles are intermittent: Quiescent periods, when the particles simply "rattle" in their nearest-neighbor cages, are interrupted by abrupt "avalanches," where a subset of particles undergo large rearrangements. Second, we find that crystallization is associated with these avalanches but that the connection is not straightforward. The amount of crystal in the system increases during an avalanche, but most of the particles that become crystalline are different from those involved in the avalanche. Third, the occurrence of the avalanches is a largely stochastic process. Randomizing the velocities of the particles at any time during the simulation leads to a different subsequent series of avalanches. The spatial distribution of avalanching particles appears random, although correlations are found among avalanche initiation events. By contrast, we find that crystallization tends to take place in regions that already show incipient local order.

colloidal glasses | ordered solid | amorphous solid | dynamic heterogeneities

Glasses are formed from the supercooled liquid state when motion is arrested on the scale of the particle diameter. Such states are thermodynamically unstable and may crystallize during, or shortly after, the initial quench. (This is the usual fate of so-called "poor" glass formers.)

Computer simulations have shown that, in such cases, crystallization readily proceeds by a sequence of stochastic micronucleation events that enhance the mobility in neighboring areas, leading to a positive feedback for further crystallization (1). Importantly, however, crystallization can also arise in mature, well-formed glasses after a long period of apparent stability. The microscopic mechanism of this process, known as "devitrification," remains elusive. Here, we simulate the dynamics of a mature hard-sphere glass and find that crystallization is associated with a series of discrete avalanche-like events characterized by a spatiotemporal burst of particle displacements on a subdiameter scale. The locations of these avalanches cannot be predicted from the prior structure of the glass, and they vary among replicate runs that differ only in initial particle velocities. Each avalanche leads to a sharp increase in crystallinity, but remarkably the crystallizing particles are primarily not those that participated in the avalanche itself. Instead, they tend to lie in nearby regions that are already partially ordered. We argue that a structural propensity to crystallize in these regions is converted into actual crystallinity by small random disturbances provided by the displacement avalanche. Although spontaneous rather than externally imposed, this pathway may relate to designed crystallization protocols such as oscillatory shear.

Devitrification is a phenomenon of both fundamental interest (2, 3) and practical importance (4–10). Indeed, the prediction and avoidance or control of devitrification represent major formulation issues in materials science, arising for both metallic (4–6) and network glasses (7, 8) as well as glass ceramics (9, 10). So far, however, there is limited understanding of the mechanisms whereby an apparently deeply arrested amorphous material can transform itself into a crystalline packing without the large-scale, diffusive particle motions whose absence [stemming from the formation of cages (11)] is a defining property of glasses.

To gain such a mechanistic understanding, we study here by molecular-dynamics (MD) simulation what is probably the simplest model of a glass: a metastable, amorphous assembly of equal-sized hard spheres in thermal motion. These systems undergo a glass transition at a volume fraction of $\phi = \phi_g \simeq 0.585$ (12). However, when the glass is prepared by rapid compression to a density just above ϕ_g, crystallites develop and grow almost immediately (1, 12). Put differently, monodisperse glasses normally crystallize before reaching maturity, where we define "maturity" by persistence of the glass for decades beyond the molecular time. This has so far precluded using hard spheres as a model system for studying the devitrification of a mature glass.

Recently, however, we have shown that mature monodisperse glasses can be created by a numerical protocol called "constrained aging" (13), in which motions that increase the global crystallinity are actively suppressed. This protocol can be viewed as selecting only the minority of dynamic trajectories in which the fresh (newly quenched) glass accidentally outlives the quench.

In what follows, we present MD results for crystallization in these mature glasses at $\phi = 0.61$. This enables us to give a detailed mechanistic analysis of the devitrification process, in what

Significance

Glasses are formed from the supercooled liquid state when motion is arrested on the scale of the particle diameter. Such states are thermodynamically unstable: An apparently deeply arrested amorphous material can transform into a crystal (devitrification) without large-scale particle motion. The prediction and avoidance of devitrification represent major formulation issues in materials science, hence the importance of understanding its mechanism. Using molecular-dynamics simulations, we study the crystallization of the simplest glass-forming system, a hard-sphere glass. We find that crystallization is caused by a subset of particles cooperatively undergoing large rearrangements in an intermittent stochastic fashion (avalanches). Particles involved in an avalanche are not themselves crystallizing, but they induce crystallization in nearby regions that already show incipient local order.

Author contributions: E.S., C.V., E.Z., W.C.K.P., M.E.C., and P.N.P. designed research; E.S., C.V., and E.Z. performed research; E.S., C.V., and E.Z. contributed analytic tools; E.S., C.V., and E.Z. analyzed data; and E.S., C.V., M.E.C., and P.N.P. wrote the paper.

The authors declare no conflict of interest.

This article is a PNAS Direct Submission.

[1]E.S. and C.V. contributed equally to this work.

[2]To whom correspondence should be addressed. E-mail: cvaleriani@quim.ucm.es.

This article contains supporting information online at www.pnas.org/lookup/suppl/doi:10.1073/pnas.1308338110/-/DCSupplemental.

is arguably the simplest model system available. We work at fixed volume (1, 12, 13) to match the conditions in colloidal glasses, which are the nearest experimental realization of the hard-sphere model system and have long formed a key testing ground for glass physics concepts (11, 14).

Our first finding is that particle dynamics in a mature glass are intermittent: quiescent periods of intracage motion are punctuated by "avalanches" in which a correlated subset of particles undergo cage-breaking displacements. Dynamic heterogeneities in glasses (15–21) [as opposed to supercooled liquids (22–27)] have been reported previously, but avalanches have not been investigated in detail and no link has yet been made with crystallization dynamics. Importantly, therefore, our second finding is that crystallization is intimately associated with these avalanches. This connection is, however, subtle: crystallinity increases during the avalanche, but most of the crystallizing particles are not among those taking part in the avalanche itself. Third, both the avalanche sequence and final crystallization pattern are stochastically determined: they depend not only on the initial particle coordinates but on their velocities, and change if these are reassigned (following ref. 28) in midsimulation. Finally, we nevertheless find that crystallization preferentially occurs in regions already showing semicrystalline correlations or "medium-range crystalline order" (MRCO) (29–31).

Although certain of the above features can be individually discerned in our previous study of crystallization in fresh glasses (1), only for mature glasses, which evolve more slowly, is the chain of causality between these events resolvable.

Results

Avalanches. Using the constrained aging method (13), we generated a mature monodisperse hard-sphere glass of $\phi = 0.61$. This had an initially low crystallinity, $X(0) \approx 1\%$, where crystallinity $X(t)$ is defined as the fraction of solid-like particles (the latter identified as described in *Materials and Methods*). Starting from the same initial particle coordinates, we launched 15 MD runs, each having a different random (Maxwellian) set of particle momenta. We have repeated the procedure for different starting configurations, all producing similar results.

In Fig. 1*A*, we show the growth of crystallinity $X(t)$ for these 15 trajectories. One might expect that, because crystallization in a glass takes place with only small (subdiameter) particle motions (1), its course should depend only on the starting configuration of the particles and not on their velocities. However, Fig. 1*A* shows that the 15 replicas have strongly dissimilar $X(t)$ profiles. This establishes a key role for stochasticity in the devitrification of mature glasses, like that reported previously for the crystallization of freshly formed ones (1). However, the $X(t)$ curves seen here for devitrification differ qualitatively from those of fresh glasses (figure 1*A* of ref. 1), which show slow monotonic growth from the beginning of the run. By contrast, in the mature samples, $X(t)$ stays constant for between two and five decades of time (measured in microscopic units; *Materials and Methods*) before steep upward jumps in $X(t)$ are seen. (These features depend on system size, as we discuss later.) Because the crystal is locally denser than the glass, each such upward step in $X(t)$ increases the free volume and speeds the approach of the next step. Under this feedback, the system finally crystallizes catastrophically and $X(t)$ goes rapidly to 1.

Key mechanistic insights are gained when we analyze one of these step-like crystallization events in more detail. The black curve in Fig. 1*B* is a close-up of the crystallinity jump shown in the black curve of Fig. 1*A* at $t \approx 2.2 \times 10^5$. The mean-square displacement (MSD) (*Materials and Methods*) is also plotted (red curve). First, we notice that $X(t)$ and the MSD are strongly correlated: both quantities jump simultaneously. To understand the MSD jump, we compute displacement vectors **u** of individual particles over chosen time intervals Δt and select those with

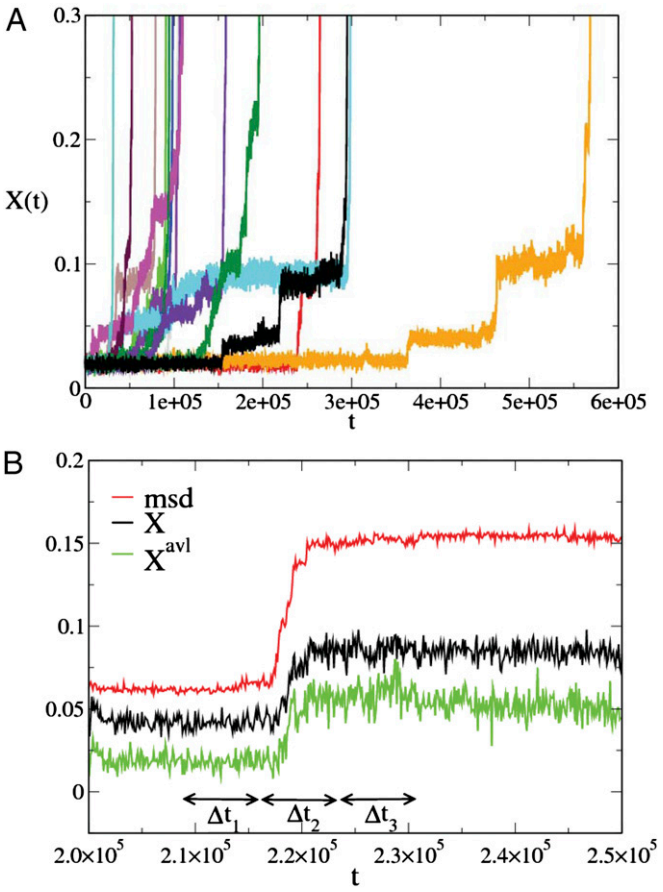

Fig. 1. (*A*) Fraction of solid-like particles $X(t)$ versus time for a system of equal-sized hard spheres at volume fraction $\phi = 0.61$. Fifteen trajectories are started from the same spatial configuration of particles but with different randomized momenta. (*B*) Crystallinity X (in black) and MSD (in red) versus time around the step-like crystallization event shown in the black curve of Fig. 1 at $t \approx 2.2 \cdot 10^5$. The green curve, X^{avl}, is the fraction of avalanche particles defined in time interval Δt_2 that are solid-like.

$|\mathbf{u}| > \sigma/3$, with σ the particle diameter σ. (This threshold is justified in *SI Appendix*.)

Fig. 2 shows these vectors as red arrows for the time windows indicated in Fig. 1*B*. In window Δt_1, the system is largely immobile; most particles rattle locally in their cages and less than 1% undergo significant displacements. During window Δt_2, which spans the jump, a burst of displacements is recorded, with around 25% of all particles moving more than $\sigma/3$. After the jump (window Δt_3), the system returns to quiescence, with again less than 1% of all particles moving significantly. We call such a sequence an "avalanche" and denote those particles that move by more than $\sigma/3$ during the jump "avalanche particles" (see *SI Appendix* for a justification of this cutoff alongside a more quantitative statistical analysis of the avalanches). It is clear from the red arrows in the second frame of Fig. 2 that these particles are not homogeneously distributed, but cluster into "avalanche regions," resembling in exaggerated form the milder dynamic heterogeneities often reported on the fluid side of the glass transition (32–34).

By interrogating the dynamics across narrower time intervals, we have observed that avalanches start to build in localized regions, then grow to peak activity, and finally die out (Movie S1). From start to finish, an avalanche typically takes about 7×10^3 time units. Highly cooperative movements can be seen during the main avalanche phase, including particles moving in

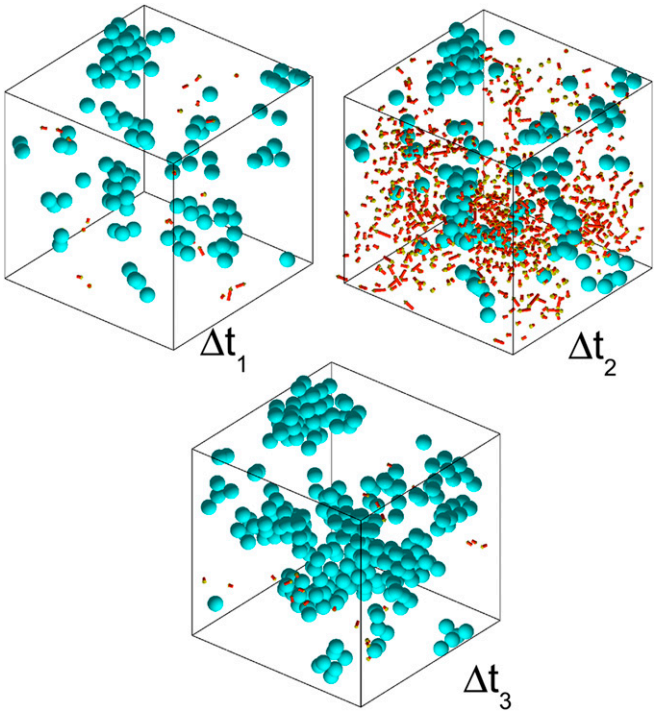

Fig. 2. Displacement vectors with modulus larger than $\sigma/3$ (red arrows with yellow heads) and solid-like particles (turquoise spheres) for time intervals Δt_1, Δt_2, and Δt_3 shown in Fig. 1*B*. The lengths of the arrows correspond to the modulus of the displacements. Solid-like particles are defined at the beginning of each time interval.

rows or circles (Fig. 3). Turquoise spheres in Fig. 2 correspond to solid-like particles. As expected from Fig. 1*B*, the avalanche leaves behind an increased population of solid-like particles.

Avalanches Mediate Crystallization. Figs. 1*B* and 2 show one representative example of a jump in crystallinity partnered with a displacement avalanche. This is a general phenomenon: in none of the runs do we see crystallinity jumps that are not associated with avalanches. The question thus arises: do avalanches cause crystallization, or vice versa? If avalanches cause crystallization, one obvious hypothesis is that the particles that move to become crystalline are the ones that form the avalanche. However, this hypothesis can be ruled out by visually inspecting Fig. 2 and realizing that there is no clear overlap between avalanche regions and regions where new crystalline particles appear. The fraction of crystalline particles is $\simeq 4\%$ before the avalanche and $\simeq 9\%$ afterward. Of the new crystalline particles, only 25% were directly involved in the avalanche, as one can infer from the green curve in Fig. 1*B*. (The proportion depends somewhat on the exact threshold of displacement used to define avalanche particles.) We conclude that the particles that crystallize are mainly not the ones that participated in the avalanche.

An alternative hypothesis is that avalanches are caused by crystallization in the sense of being triggered by the small rearrangements ($|\mathbf{u}| < \sigma/3$) (12, 13) needed to achieve local crystallinity. If so, avalanches would be absent whenever crystallization is suppressed by size polydispersity. Fig. 4*A* shows the MSD and $X(t)$ of a glass with 6% polydispersity at volume fraction $\phi = 0.60$. As expected from our earlier work (12, 35), the crystallinity stays flat throughout the run; yet we see that the MSD jumps in a way that, by the methods already described, can be identified as avalanches. Moreover, avalanche-like dynamic heterogeneity (in less extreme form) was previously seen for other noncrystallizing glassy systems in 2D and 3D simulations (16, 18, 19, 22, 24, 25) and in colloid experiments (36, 37). Therefore, we can discard the hypothesis that crystallization causes avalanches, rather than vice versa.

The stochastic nature of avalanches was already shown in Fig. 1, where the trajectory of each replica has a different crystallinity evolution $X(t)$. A further illustration is given in Fig. 4*B*, where we compare a trajectory undergoing an avalanche with three systems started from a common configuration just before the avalanche. Each replica is launched with a different set of particle velocities, and in all three cases the avalanche is averted. This finding shows that the triggering of an avalanche from the quiescent state does not depend on particle coordinates alone, but rather on the appearance of a successful combination of positions and momenta. We speculate that these rare events involve emergence of cooperative motions such as those illustrated in Fig. 3. In contrast, if velocities are reassigned midway through an avalanche (Fig. 4*B*), the avalanche does not stop, but continues along an altered path. This implies that the "activated" state is structurally distinguishable from the quiescent one, although we have not yet found a clear static signature for it.

The requirement of an unlikely combination of positions and velocities to trigger an avalanche, combined with the fact that avalanches cause crystallinity to grow (explored further below), explains the stochasticity of devitrification in our mature samples and is likely also implicated in the stochastic crystallization in fresh glasses (1). That displacement avalanches mediate crystallization in hard-sphere glasses is the central finding of this paper.

Heterogeneities. As previously stated, the different trajectories in Fig. 1 lead to different final crystallization patterns from the same initial configuration. Visual inspection of these patterns shows only limited similarity between them. Nonetheless, one might expect some regions to be more likely to crystallize than others. The crystallization propensity is assessed by superimposing the crystalline particles (XP) of all trajectories as these

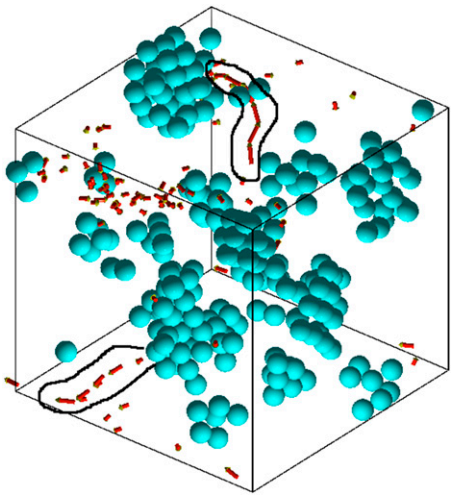

Fig. 3. Displacement field for a typical avalanche in which cooperative motion where particles follow each other are highlighted.

first cross a fixed crystallinity threshold (we choose $X = 0.1$). To quantify any heterogeneity in the resulting superimposition, we divide the simulation box in $3 \times 3 \times 3$ equal subvolumes and evaluate the density in each, normalizing by the overall density. The resulting normalized densities, $\hat{\rho}_i = \rho_i/\rho$, are plotted as a function of subvolume index in Fig. 5*A*. By computing the

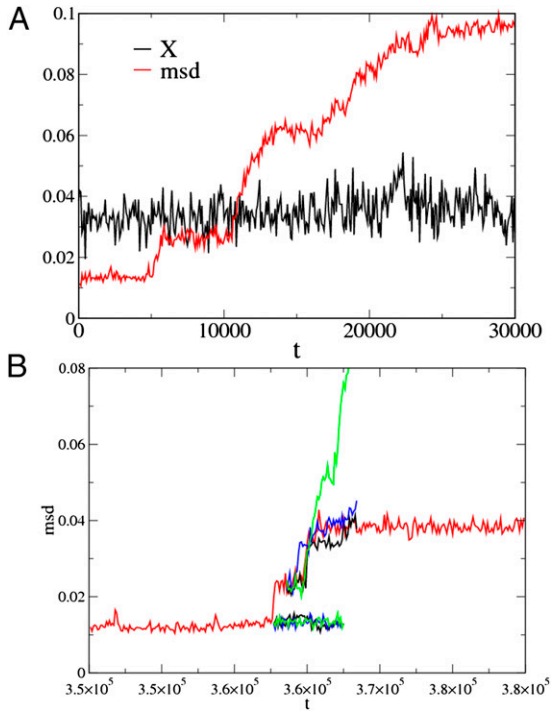

Fig. 4. (*A*) Crystallinity $X(t)$ (black) and MSD (red) versus time for a 6% polydisperse system at $\phi = 0.60$. (*B*) Red curve: MSD versus time for a trajectory of the monodisperse system showing an avalanche. Blue, green, and black curves: MSDs for the same system when the particle velocities are randomized immediately before the avalanche and in the middle of the avalanche.

fluctuations of $\hat{\rho}_i$ around the average value, 1, we get a quantitative measure of the degree of heterogeneity, $h_d = \langle \hat{\rho}_i^2 \rangle - \langle \hat{\rho}_i \rangle^2$. For crystalline particles in our replicated runs, we find $h_d = 0.22$, more than four times above the background level, $h_d = 0.050$, computed by superposing crystalline particles for 15 runs starting from independent initial configurations rather than from the same one. We can conclude that there are some regions in the initial configuration that are more prone to crystallize than others. It has been found in supercooled liquids that these regions correlate with a partial ordering known as MRCO, which is quantified by an averaged local bond order parameter $\overline{q}_6$ (30, 31, 38). Fig. 5*A* compares the density of XP particles in our simulations with the density of MRCO, identified as those particles with $\overline{q}_6$ in the top 10%. As with the earlier work on supercooled liquids (30, 31), there is a clear, although not complete, correlation between MRCO in the initial configuration and subsequent crystallization.

We also investigate whether there are regions where avalanches have a higher propensity to take place by doing a similar analysis as that described above but for particles involved in the first avalanche (AP) instead. As seen in Fig. 5*B*, the density of these particles shows only small variations between subvolumes, suggesting that avalanches occur almost at random throughout the system in mature glasses (whereas the crystallinity induced by these avalanches has a significantly higher propensity to appear in some regions than in others).

It has been found that dynamic heterogeneities in supercooled fluids, involving large-scale rearrangement of the particle positions (the α process), tend to grow from regions of high displacement in low-frequency quasilocalized phonon modes (so-called soft spots) (18, 23, 39–41). In view of our result that avalanches occur almost at random throughout the system, one would be tempted to conclude that avalanches and dynamic heterogeneities are fundamentally different dynamic events. However, a closer study does reveal a clear correlation across trajectories among avalanche initiator particles (AIP) (those involved in the first steps of avalanche formation). In fact, the density heterogeneities plot of AIP shown in Fig. 5*B* shows large density variations between subboxes (in *SI Appendix*, we show that this is a statistically significant result). Therefore, AIP and dynamic heterogeneities share the tendency to develop in certain regions of the system. Whether or not these regions also correspond to soft spots for the case of mature glasses requires further investigation beyond the scope of this paper. Nevertheless, we show some preliminary analyses in *SI Appendix*, alongside a more detailed account of heterogeneities, including pictorial representations.

Discussion and Conclusions

We have investigated the mechanism by which crystals develop in amorphous glasses composed of equal-sized hard spheres. In contrast with our previous work on freshly prepared samples, we addressed here mature glasses, whose arrest is characterized by a MSD that stays flat for several decades in time before the onset of crystallization. We have shown that crystallization is intimately associated with particle displacement avalanches (Figs. 1*B* and 2) and that crystallization is caused by these avalanches and not vice versa. However, the majority of avalanche participants do not become crystalline (green curve in Fig. 1*B*), and most crystallizing particles move little during the avalanche. Thus, the displacement avalanche is not, of itself, the sequence of motions needed to transform an amorphous region into crystal.

Instead, avalanches within the mature glass appear to be autonomous structural rearrangements, involving cooperative particle motion. These mesoscopic avalanches have a strongly stochastic character, and are triggered by unlikely local combinations of particle positions and momenta. An individual avalanche can be averted entirely by reassigning momenta just before its inception; once underway, however, such reassignment only diverts it along a different path (Fig. 4). Although no obvious propensity to occur in particular positions can be seen in

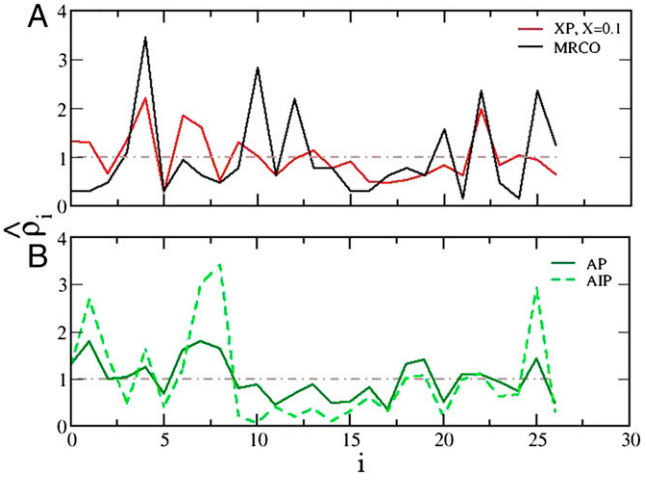

Fig. 5. Normalized density, ρ_i, as a function of the index i identifying each subvolume of the simulation box for various particle types (see text). (*A*) Red: crystalline particles (XP) are those of all of the trajectories in Fig. 1*A* as they first cross the crystallinity threshold X = 0.1. Black: medium-range crystalline order (MRCO) particles are those in the initial configuration with bond order parameter $\overline{q}_6$ in the top 10%. (*B*) Dark green (solid line): avalanche particles (AP) are those participating in the first avalanche of all trajectories. Light green (dashed line): avalanche initiator particles (AIP) are those involved in initiating the first avalanche of all trajectories as defined in *SI Appendix*.

the statistics of avalanche participants, this can be detected among AIP. This finding implies a correlation with static structure (explored further in *SI Appendix*), possibly including "soft spots" of the type known to be linked to dynamic heterogeneity in supercooled liquids (18, 39, 40) and some glasses (18, 23, 41). If so, our avalanches might be viewed as a limiting type of dynamic heterogeneity, arising as the system's density or age increases so that activity becomes rare. However, the stochastic character of the avalanches might also be taken as support for suggestions (18, 24) that a qualitatively different type of dynamics takes over in systems, such as ours, that are deep into the glassy state. In addition, and in common with supercooled liquids, we find that the crystals tend to grow in regions of MRCO [which seem to be themselves anticorrelated with the soft spots (29–31); *SI Appendix*, Fig. S8].

The likely role of avalanches in crystallization is to create the small disturbances required to accomplish ordering in regions that, as noted above, already have a propensity to crystallize. Avalanche-induced disturbances might shake a nearly ordered region into order, but could also facilitate growth of an established crystallite at its perimeter. This avalanche-mediated mechanism for devitrification somewhat resembles the breakdown dynamics of an attractive colloidal gel (42). The process could also be closely related to protocols such as shearing in which mature glasses are induced to crystallize by gentle agitation (43–45). In contrast to those protocols, here the required agitation is spontaneously generated. Indeed, the intrinsic avalanche dynamics remain present even when crystallization itself is prevented by polydispersity.

In keeping with previous findings for fresh glasses (1, 12), the ordering induced by an avalanche reduces the pressure in the system and creates positive feedback for further avalanches. This process gives rise to a nontrivial system size dependence for the time evolution of global properties such as the mean crystallinity, as explained in *SI Appendix*. However, it does not qualitatively change the mesoscopic mechanism of avalanche-mediated devitrification that we have described.

To confirm that our findings are not some special feature of systems prepared by constrained aging, we have additionally performed simulations on fresh glasses prepared by rapid compression to a higher concentration, $\phi = 0.62$, where there is no need to resort to constrained aging to obtain a mature glass. We found that these glasses show similar behavior to that reported above for the constrained-aged systems at $\phi = 0.61$: long quiescent periods and sudden coincident jumps in the crystallinity and MSD (*SI Appendix*). Therefore, this devitrification mechanism is evident for mature glasses, either prepared by constrained aging ($\phi = 0.61$) or by quick compression ($\phi = 0.62$). By contrast, a glass prepared by quick compression at $\phi = 0.61$ (1) crystallizes while still fresh and does not clearly show the avalanche mechanism.

Our work suggests several avenues for future research. One is to study hard-sphere devitrification at constant pressure. A second is to address by our methods mixtures of different-sized hard spheres. This would represent a first step toward modeling bulk metallic glasses, which are generally multicomponent alloys (46, 47). Mechanistic insights along the lines pursued in this paper might then shed light on the devitrification of such glasses during processing, which is a major issue in technology (5, 6).

Materials and Methods

Simulation Details. We perform event-driven MD simulations in the *NVT* ensemble with cubic periodic boundary conditions for a system of $n = 3{,}200$ monodisperse hard spheres (48, 49). We also simulate a polydisperse system of $n = 2{,}000$ particles where the particle diameters are chosen according to a discrete Gaussian distribution with relative standard deviation $s = 0.06$. Mass, length, and time are measured in units of particle mass m, particle diameter σ (or $\bar{\sigma}$ for the polydisperse case), and $t_0 = \sqrt{m\sigma^2/\kappa_B T}$, where κ_B is the Boltzmann constant and T is the temperature, and we set $\kappa_B T = 1$. The packing fraction is defined as $\phi = \frac{\pi}{6} N\sigma^3/V$ (with V the system's volume).

To generate the initial configuration, we follow the "constrained aging" procedure described previously (13). We use a configuration resulting from constrained aging as a starting point for unconstrained MD runs.

Analysis Details. The MSD is calculated as $\frac{1}{N}\sum_{i=1}^{N}(\mathbf{r}_i(t) - \mathbf{r}_i(0))^2$, where $\mathbf{r}_i$ is the position of particle i.

The crystallinity, X, is defined as the number of solid-like particles divided by the total number of particles. As in previous work (35), we identify solid-like particles according to a rotationally invariant local bond order parameter d_6 (50, 51). To compute it, we first identify the number of neighbors $N_b(i)$ of each particle i using the parameter-free SANN algorithm (52). Next, for every particle i, we compute the complex vector $\mathbf{q}_6$ whose components are given by $q_{6m}(i) = \frac{1}{N_b(i)}\sum_{j=1}^{N_b(i)} Y_{6m}(\theta_{ij},\phi_{ij})/(\sum_{m=-6}^{6} q_{6m}(i)\cdot q_{6m}^{*}(i))^{1/2}$ (with $m \in [-6,6]$), where Y_{6m} are sixth-order spherical harmonics. Then we compute the rotationally invariant bond order parameter d_6 by calculating the scalar product between each particle's $\mathbf{q}_6$ and its neighbors, $d_6(i,j) = \sum_{m=-6}^{6} q_{6m}(i)\cdot q_{6m}^{*}(j)$, and consider particles i and j as having a "solid connection" if their $d_6(i,j)$ exceeds the value of 0.7. A particle is labeled as solid-like if it has at least six solid connections.

ACKNOWLEDGMENTS. C.V. and E.S. acknowledge financial support from an Intra-European Marie Curie Fellowship (in Edinburgh; 237443-HINECOP-FP7-PEOPLE-IEF-2008 and 237454-ACSELFASSEMBLY-FP7-PEOPLE-IEF-2008, respectively) and from a Marie Curie Career Integration Grant (322326-COSAACFP7-PEOPLE-CIG-2012 and 303941-ANISOKINEQ-FP7-PEOPLE-CIG-2011, respectively), together with the Juan de La Cierva (JCI-2010-06602) and Ramon y Cajal (RYC-2010-06098) Spanish Fellowships and Spanish National Project FIS2010-16159. E.Z. acknowledges support from the FIRB program of the Ministero dell' Istruzione, dell'Universita' e della Ricerca through the project ANISOFT (RBFR125H0M). W.C.K.P., M.E.C., and E.Z. acknowledge support from ITN-234810-COMPLOIDS, and W.C.K.P. and M.E.C. from the Engineering and Physical Sciences Research Council Grant EP/J007404. M.E.C. holds a Royal Society Research Professorship. This work has made use of the resources provided by the Edinburgh Compute and Data Facility (ECDF). The ECDF is partially supported by the eScience Data Information and Knowledge Transformation initiative.

1. Sanz E, et al. (2011) Crystallization mechanism of hard sphere glasses. *Phys Rev Lett* 106(21):215701.
2. Zanotto ED (2013) *Crystals in Glass: A Hidden Beauty* (Wiley-American Ceramic Society, Hoboken, NJ).
3. Kelton KF (1991) Crystal nucleation in liquids and glasses. *Solid State Physics*, eds Ehrenreich H, Turnbull D (Academic, Boston), Vol 45, pp 75–178.
4. Kulik T (2001) Nanocrystallization of metallic glasses. *J Non-Cryst Solids* 287:145–161.
5. Schroers J (2010) Processing of bulk metallic glass. *Adv Mater* 22(14):1566–1597.
6. Schroers J (2013) Bulk metallic glasses. *Phys Today* 66:32–37.
7. Marshall RR (1961) Devitrification of natural glass. *Geol Soc Am Bull* 72:1493–1520.
8. Ellison A, Minelly J (2002) New materials for optical amplifiers. *Optical Fiber Telecommunications IV-A: Components*, eds Kaminov I, Tingye L (Academic, Boston), pp 80–173.
9. Rawlings RD, Wu JP, Boccaccini AR (2006) Glass-ceramics: Their production from wastes—a review. *J Mater Sci* 41:733–761.
10. Höland W, Beall GH (2012) *Glass Ceramic Technology* (Wiley, Hoboken, NJ).
11. Pusey PN, van Megen W (1987) Observation of a glass transition in suspensions of spherical colloidal particles. *Phys Rev Lett* 59(18):2083–2086.
12. Zaccarelli E, et al. (2009) Crystallization of hard-sphere glasses. *Phys Rev Lett* 103(13): 135704.
13. Valeriani C, et al. (2011) Crystallization and aging in hard-sphere glasses. *J Phys Condens Matter* 23(19):194117.
14. Hunter GL, Weeks ER (2012) The physics of the colloidal glass transition. *Rep Prog Phys* 75(6):066501.
15. Miyagawa H, Hiwatari Y, Bernu B, Hansen JP (1988) Molecular dynamics study of binary soft-sphere mixtures: Jump motions of atoms in the glassy state. *J Chem Phys* 88:3879.
16. Kob W, Barrat J-L (2000) Fluctuations, response and aging dynamics in a simple glass-forming liquid out of equilibrium. *Eur Phys J B* 13:319.
17. Saltzman EJ, Schweizer KS (2008) Large-amplitude jumps and non-Gaussian dynamics in highly concentrated hard sphere fluids. *Phys Rev E Stat Nonlin Soft Matter Phys* 77(5 Pt 1):051504.
18. Brito C, Wyart M (2009) Geometric interpretation of previtrification in hard sphere liquids. *J Chem Phys* 131(2):024504.
19. El Masri D, Berthier L, Cipelletti L (2010) Subdiffusion and intermittent dynamic fluctuations in the aging regime of concentrated hard spheres. *Phys Rev E Stat Nonlin Soft Matter Phys* 82(3 Pt 1):031503.
20. Vollmayr-Lee K, Baker EA (2006) Self-organized criticality below the glass transition. *Europhys Lett* 76:1130.
21. Yunker P, Zhang Z, Aptowicz KB, Yodh AG (2009) Irreversible rearrangements, correlated domains, and local structure in aging glasses. *Phys Rev Lett* 103(11):115701.

22. Büchner S, Heuer A (2000) Metastable states as a key to the dynamics of supercooled liquids. *Phys Rev Lett* 84(10):2168–2171.
23. Widmer-Cooper A, Perry H, Harrowell P, Reichman DR (2008) Irreversible reorganization in a supercooled liquid originates from localized soft modes. *Nat Phys* 4:711–715.
24. Candelier R, et al. (2010) Spatiotemporal hierarchy of relaxation events, dynamical heterogeneities, and structural reorganization in a supercooled liquid. *Phys Rev Lett* 105(13):135702.
25. Keys AS, Hedges LO, Garrahan JP, Glotzer SC, Chandler D (2011) Excitations are localized and relaxation is hierarchical in glass-forming liquids. *Phys Rev X* 1:021013.
26. Kawasaki T, Onuki A (2013) Slow relaxations and stringlike jump motions in fragile glass-forming liquids: Breakdown of the Stokes-Einstein relation. *Phys Rev E Stat Nonlin Soft Matter Phys* 87(1):012312.
27. Appignanesi GA, Rodriguez Fris JA (2009) Space and time dynamical heterogeneity in glassy relaxation. The role of democratic clusters. *J Phys Condens Matter* 21(20): 203103–203116.
28. Widmer-Cooper A, Harrowell P, Fynewever H (2004) How reproducible are dynamic heterogeneities in a supercooled liquid? *Phys Rev Lett* 93(13):135701.
29. Kawasaki T, Araki T, Tanaka H (2007) Correlation between dynamic heterogeneity and medium-range order in two-dimensional glass-forming liquids. *Phys Rev Lett* 99(21):215701.
30. Kawasaki T, Tanaka H (2010) Formation of a crystal nucleus from liquid. *Proc Natl Acad Sci USA* 107(32):14036–14041.
31. Kawasaki T, Tanaka H (2010) Structural origin of dynamic heterogeneity in three-dimensional colloidal glass formers and its link to crystal nucleation. *J Phys Condens Matter* 22(23):232102.
32. Kob W, Donati C, Plimpton SJ, Poole PH, Glotzer SC (1997) Dynamical heterogeneities in a supercooled Lennard-Jones liquid. *Phys Rev Lett* 79:2827–2830.
33. Ediger MD (2000) Spatially heterogeneous dynamics in supercooled liquids. *Annu Rev Phys Chem* 51:99–128.
34. Berthier L, Biroli L, Bouchaud JP, Cipelletti L, Van Saarloos W (2011) *Dynamical Heterogeneities in Glasses, Colloids, and Granular Media* (Oxford Univ Press, Oxford).
35. Pusey PN, et al. (2009) Hard spheres: Crystallization and glass formation. *Philos Trans A Math Phys Eng Sci* 367(1909):4993–5011.
36. Cipelletti L, Bissig H, Trappe V, Ballesta P, Mazoya S (2003) Time-resolved correlation: A new tool for studying temporally heterogeneous dynamics. *J Phys Condens Matter* 15:S257.
37. Fris JAR, Appignanesi GA, Weeks ER (2011) Experimental verification of rapid, sporadic particle motions by direct imaging of glassy colloidal systems. *Phys Rev Lett* 107(6):065704.
38. Lechner W, Dellago C (2008) Accurate determination of crystal structures based on averaged local bond order parameters. *J Chem Phys* 129(11):114707.
39. Widmer-Cooper A, Harrowell P (2006) Predicting the long-time dynamic heterogeneity in a supercooled liquid on the basis of short-time heterogeneities. *Phys Rev Lett* 96(18):185701.
40. Widmer-Cooper A, Perry H, Harrowell P, Reichman DR (2009) Localized soft modes and the supercooled liquid's irreversible passage through its configuration space. *J Chem Phys* 131(19):194508.
41. Chen K, et al. (2011) Measurement of correlations between low-frequency vibrational modes and particle rearrangements in quasi-two-dimensional colloidal glasses. *Phys Rev Lett* 107(10):108301.
42. Cipelletti L, Manley S, Ball RC, Weitz DA (2000) Universal aging features in the restructuring of fractal colloidal gels. *Phys Rev Lett* 84(10):2275–2278.
43. van Megen W, Underwood SM (1993) Change in crystallization mechanism at the glass transition of colloidal spheres. *Nature* 362:616–618.
44. Haw MD, Poon WCK, Pusey PN (1998) Direct observation of oscillatory-shear-induced order in colloidal suspensions. *Phys Rev E* 57:6859.
45. Koumakis N, Schofield AB, Petekidis G (2008) Effects of shear induced crystallization on the rheology of hard sphere colloids. *Soft Matter* 4:2008–2018.
46. Ruta B, Baldi G, Monaco G, Chushkin Y (2013) Compressed correlation functions and fast aging dynamics in metallic glasses. *J Chem Phys* 138(5):054508.
47. Baldi G, et al. (2013) Emergence of crystal-like atomic dynamics in glasses at the nanometer scale. *Phys Rev Lett* 110(18):185503.
48. Rapaport DC (1995) *The Art of Molecular Dynamics Simulation* (Cambridge Univ Press, Cambridge, UK).
49. Zaccarelli E, et al. (2002) Confirmation of anomalous dynamical arrest in attractive colloids: A molecular dynamics study. *Phys Rev E* 66(4 Pt 1):041402.
50. Steinhardt PJ, Nelson DR, Ronchetti M (1983) Bond-orientational order in liquids and glasses. *Phys Rev B* 28:784.
51. Auer S, Frenkel D (2001) Prediction of absolute crystal-nucleation rate in hard-sphere colloids. *Nature* 409(6823):1020–1023.
52. van Meel JA, Filion L, Valeriani C, Frenkel D (2012) A parameter-free, solid-angle based, nearest-neighbor algorithm. *J Chem Phys* 136(23):234107.

Supporting Information to "Avalanches mediate crystallization in a hard-sphere glass"

E. Sanz[1], C. Valeriani[1], E. Zaccarelli[2], W. C. K. Poon[3], M. E. Cates[3] and P. N. Pusey[3]

[1]*Departamento de Química Física, Facultad de Ciencias Químicas, Universidad Complutense de Madrid, 28040 Madrid, Spain*
[2]*CNR-ISC and Dipartimento di Fisica, Università di Roma La Sapienza, P.le A. Moro 2, 00185 Roma, Italy*
[3]*SUPA, School of Physics and Astronomy, University of Edinburgh, Mayfield Road, Edinburgh, EH9 3JZ, Scotland*

I. AVALANCHE DEFINITION AND STATISTICS

We define avalanche particles as those whose displacement ($|\mathbf{u}|$) during a given time interval is larger than $\sigma/3$. To show that such displacements are indeed significantly large we compute the cumulative probability distribution of displacements in the initial quiescent plateau (before the first avalanche) for a time interval equal to the average duration of an avalanche. By inspecting the 15 trajectories shown in Fig. 1 in the main text we found that an avalanche lasts on average about $7000t_0$. (Here t_0 is the time unit introduced in the Methods section.) The black curve in Fig. 1 represents $P(|\mathbf{u}| < \alpha)$, the probability that the displacement of a particle is smaller than α, for a time interval of $7000t_0$ in the initial quiescent plateau. Clearly, displacements larger than $\sigma/3$ are extremely rare in the quiescent period, which justifies our threshold for the definition of avalanche particles. By contrast, it is not unlikely that particles travel for even longer distances during an avalanche. This is demonstrated by the red curve in Fig. 1, which corresponds to $P(|\mathbf{u}| < \alpha)$ calculated during a time interval that includes an avalanche. The curve is made with the collection of all the displacements during the first avalanche of each of the trajectories shown in Fig. 1 of the main text. About 15 per cent of the particles travel more than $\sigma/3$ during an avalanche. This means that, according to our definition, an avalanche involves on average about 500 particles. Notice that particles do not move beyond their diameter during an avalanche and only 6 percent of them travel beyond the radius. Therefore, the mobility during an avalanche, even if much larger than that during a quiescent period, is still rather restricted.

The rate at which avalanches nucleate is the limiting factor for the growth of crystals in a glass. We can estimate the avalanche nucleation rate for our configuration by counting the number of avalanches and dividing it by the time the system takes to fully crystallize and by the volume of the system. The value we get after averaging over all trajectories is $6{\cdot}10^{-9}\ \sigma^{-3}t_0^{-1}$. This nucleation rate implies that the first avalanche takes place, on average, in $6{\cdot}10^4 t_0$ in our system of volume $14^3\sigma^3$. Of course, the larger the system's volume, the shorter the time it takes for the first avalanche to nucleate.

Below we discuss the influence of the system size on the crystallization pathway, and present a more quantitative description of the avalanches than that given in the main text. This type of analysis should be interpreted with care, though. As discussed below, the qualitative picture of the crystallization mechanism is not affected by the way the configuration is generated. However, since we are dealing with a system out of equilibrium, the history of formation and, of course, the packing fraction, may have an impact over the precise value

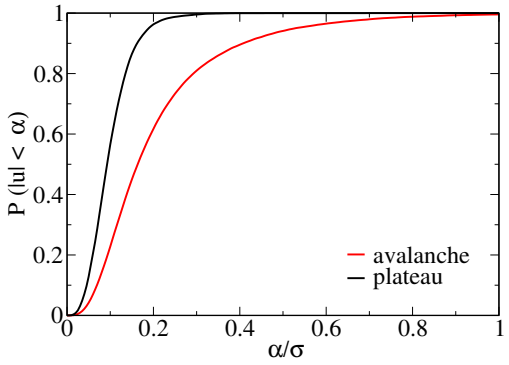

FIG. 1: Probability that the displacement of a particle is smaller than a certain distance, $P(|\mathbf{u}| < \alpha)$, versus the distance, α, in particle diameters. We compare $P(|\mathbf{u}| < \alpha)$ for a quiescent period (black) with $P(|\mathbf{u}| < \alpha)$ when an avalanche takes place (red). In the quiescent plateau, $P(|\mathbf{u}| < \alpha)$ is calculated for a time interval equal to the average duration of an avalanche ($7000t_0$).

of the variables here discussed.

II. DEPENDENCE ON SYSTEM SIZE

To check that our description of crystallization mechanism of an HS glass also applies for larger systems, we initiated a run from a large configuration made from tiling together $3\times3\times3$ copies of the configuration used as a starting point for the trajectories shown in Fig. 1a of the main text. Previous work [1] shows that the artificial periodicity induced by such spatial replication is soon lost under the randomizing influences of the momenta (which are assigned independently in each sub-box). Visual inspection shows that avalanches appear throughout the large system (Fig. 2D)).

Important differences can be seen with respect to the small system in the time evolution of the overall crystallinity and the fraction of avalanche particles. The first avalanche occurs sooner in the large system, as expected for a rare event initiated by local stochasticity, and because the feedback between avalanches and free volume is global, $X(t)$ accelerates faster thereafter. Moreover, most of the time there is at least one avalanche present so that the globally averaged fraction of avalanche particles, and with it $X(t)$, evolves much more smoothly (Fig. 2B) than in the smaller systems reported above (Fig. 2A).

On the other hand, if attention is restricted to a part of the large system (Fig. 2C) (matched in size to the smaller systems of Fig. 2A) then the dynamics of individual avalanches, including their extent and consequences for crystallization, remain qualitatively similar to before (the dynamics of supercooled fluids shows a similar system size dependence [2]). Since our mechanistic interpretation of the devitrification process is formulated at the mesoscopic scales already captured by the simulations of 3200 particles, this interpretation remains unaltered. Any further system-size-dependence of the crystallization time is not expected once the density of avalanches is higher than one per simulation box volume, which is the case in our large system.

The simulation of the replicated system allows us calculate a distribution of the size of clusters formed by avalanche particles. A cut-off distance of 1.1 particle diameters is used to identify neighbors in the same cluster and avalanche particles are defined in a time interval

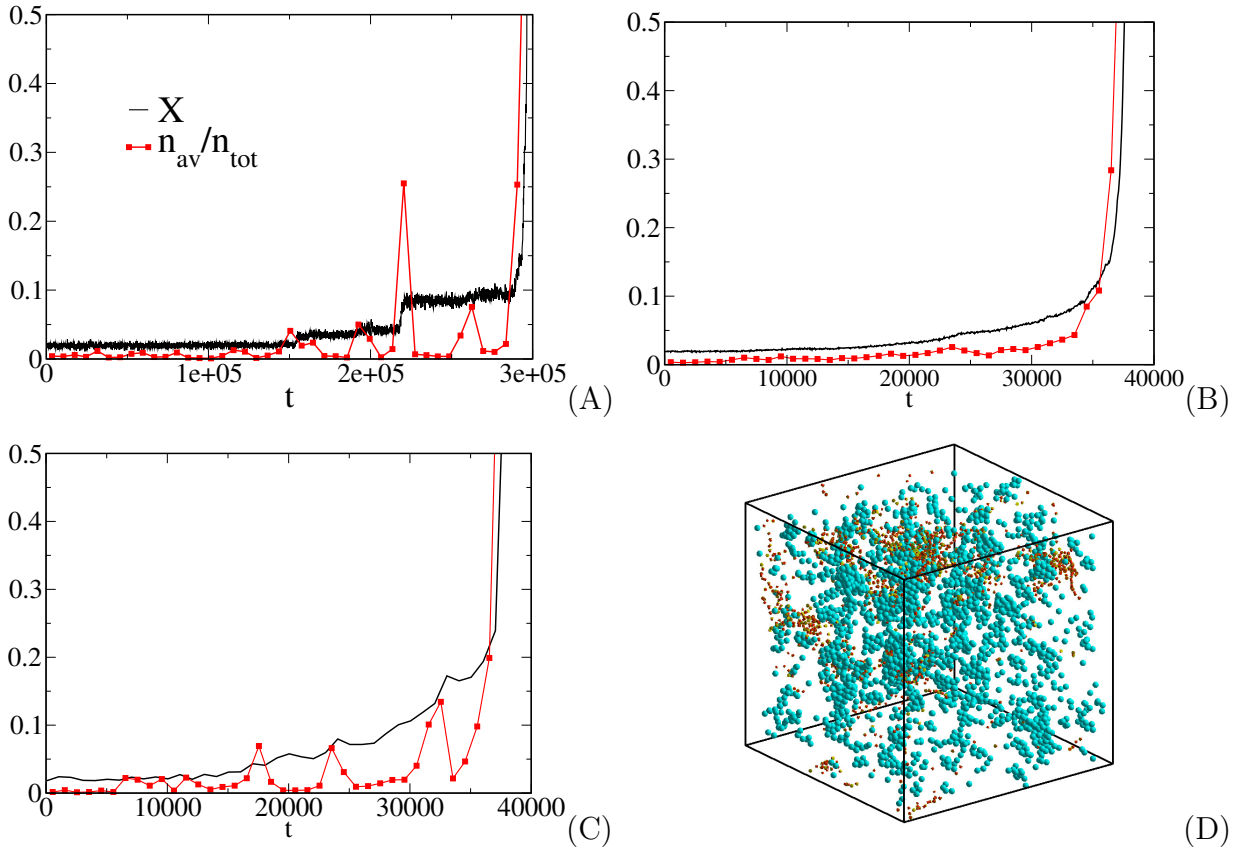

FIG. 2: Fraction of crystalline particles and of particles belonging to an avalanche as a function of time for different system sizes. Avalanche particles are defined in a time interval given by the distance between consecutive points (which depends on the case under study). (A) a 3200-particle system (black trajectory in Fig. 1a of the main text); (B) a $3 \times 3 \times 3$ replica of the 3200-particle system; (C) a cubic subset of system (B) containing ~ 3200 particles; (D) Snapshot of the large system (B) at $t = 22000t_0$. Solid-like particles are turquoise spheres and avalanche particles in $[t, (t + 1000t_0)]$ are red arrows with yellow heads.

of $500t_0$. The cluster size (number of particles) distribution is plotted in Fig. 3. Clusters as large as ~ 1000 particles are observed. The distribution of cluster sizes is typical of a random percolation, where clusters randomly appear and merge; this is shown by the -2.18 slope [3] of the cluster size distribution in the log-log plot of Fig. 3. By contrast, the size distribution of crystalline clusters found in a fresh glass at the same density has a slope of -1.7, indicating a loss of randomness due to the preferable appearance of crystalline particles in the vicinity of existing clusters [4].

We note that the $X(t)$ profile of the replicated system is qualitatively similar to that of the immature (fresh) glass investigated in Ref. [1] (Fig. 1a). Our preliminary investigations on this respect suggest that avalanches are also present in samples of fresh monodisperse hard spheres glasses, although in a less evident form. This would be consistent with the stochastic growth of crystals via micro-nucleation events described in Ref. [1].

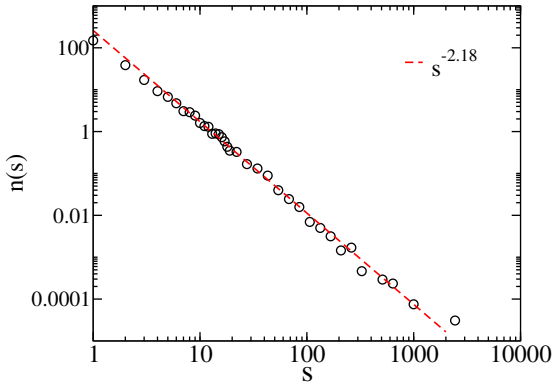

FIG. 3: Distribution of the size, s, of clusters formed by avalanche particles averaged for $X < 0.1$ (black circles). This is calculated for the large system made from tiling together $3 \times 3 \times 3$ copies of the system used in Fig. 1a of the main text. The dashed red line has a slope of -2.18 in a log-log plot, which is the expected slope for a random percolation behavior.

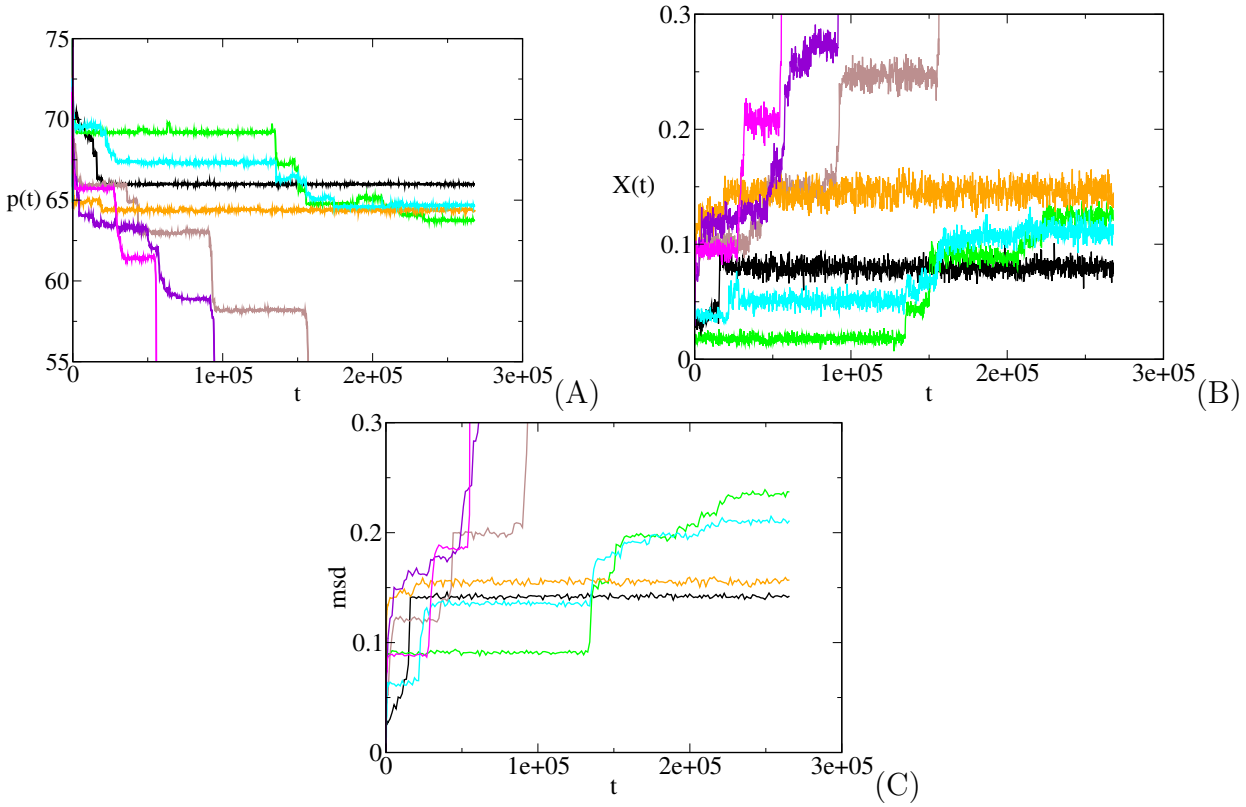

FIG. 4: Pressure (A), crystallinity X (B) and msd (C) versus time for 7 independent trajectories of a monodisperse hard spheres suspension at $\phi = 0.62$ generated by quick compression.

III. PREPARATION PROTOCOL OF THE INITIAL CONFIGURATION

The results discussed in the main text correspond to glassy configurations generated with a constrained aging algorithm [5] that prevents the appearance of crystallites as the system is compressed to its final density. In this section we show that the crystallization

mechanism described in the main text does not depend on the use of this particular protocol to generate the initial configuration. Simply by quickly compressing the system it is also possible, although less likely, to obtain dense amorphous configurations of monodisperse hard spheres that do not readily crystallize. The odds to successfully generate such configurations increase with the compressing rate and the target density. We have been able to generate by quick compression configurations at $\phi = 0.62$ that stay amorphous for a few decades before crystallizing. In Fig. 4 we show the time evolution of the pressure, the crystallinity and the mean squared displacement for 7 of these configurations. This plot is not qualitatively different from that of Fig. 1 in the main text. Crystallization jumps are correlated to jumps in the msd (avalanches). Moreover, we also show that the pressure drops in a sequence of steps, as a consequence of the more efficient packing achieved in crystallization events.

IV. CRYSTALLIZATION AND AVALANCHE PROPENSITY

In Fig. 5 we show some snapshots to give a qualitative view of the propensities analysis presented in the main text. In Fig. 5A we show a snapshot resulting from the superimposition of the crystalline particles found at $X = 0.1$ for the 15 trajectories of Fig.1a (main text). This is compared with a superimposition of the crystalline particles found at $X = 0.1$ for 15 trajectories starting from different configurations (Fig. 5F). In Fig. 5F particles are noticeably more homogeneously distributed than in Fig. 5A, which indicates that in the configuration from which the 15 runs of Fig.1a (main text) were initiated there are some regions which are more prone to crystallize than others. Figure 5E shows MRCO particles (see main text) in the initial configuration of the 15 trajectories of Fig.1a. Comparison of Fig. 5E with Fig. 5A shows some correlation between MRCO regions and those with a high propensity to crystallize, for example a high density of particles in the centre of the simulation box. Figure 5B shows a superimposition of the particles taking part of the first avalanche (AP) in each of the 15 trajectories of Fig. 1a. Differently from Fig. 5A, where there is a noticeable heterogeneity in the propensity to crystallize, here the probability to participate in an avalanche looks rather homogeneous throughout the system (density heterogeneities are comparable to those seen in the random case shown in Fig. 5F). By contrast, when we plot in Fig. 5C only those particles involved in the initiation of the first avalanche (see below) of each trajectory there is a clear heterogeneity of the distribution of such particles throughout the system. Fig. 5D shows the superimposition of the particles with the top 10% variance with respect to their average position during the initial quiescent plateau for the 15 trajectories (rattler particles (RP)). We note that there is a mild *anti*-correlation between MRCO and RP, as it has been found in supercooled liquids [6–8] (see also Fig. 8).

We have shown that crystallization in hard-sphere glasses tends to take place in regions which have a high degree of medium range crystalline order. This observation agrees with what has been found in a number of other systems in their more mobile "supercooled" liquid states, e.g. [7]. However we also found that the avalanche participants are almost randomly distributed through the sample (green solid line in Fig. 5 (b) of the main text). This, in principle, suggests that there may be distinct differences between the avalanches found in high-concentration glasses and the dynamic heterogeneity (DH) of lower-concentration supercooled liquids (in supercooled liquids, dynamic heterogeneities tend to develop with a higher probability in so-called soft spots [10]). However, closer inspection of our data reveals that avalanches are *initiated* preferentially in certain regions of the system. As explained in

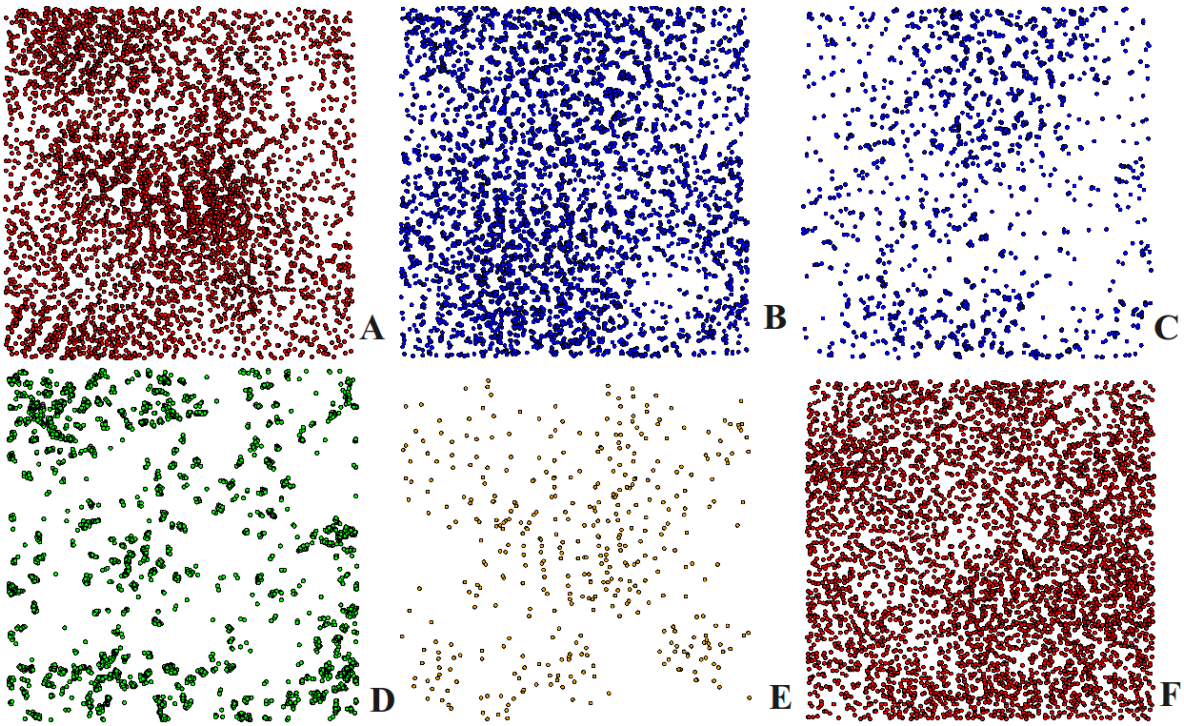

FIG. 5: A-D superimposition of different types of particles for 15 trajectories starting with different set of momenta from the configuration analysed in the main text: (A) crystalline particles at $X = 0.1$ (XP); (B) particles involved in the first avalanche (AP); (C) particles involved in the initiation of the first avalanche (AIP); (D) particles with the top 10% variance with respect to their average position during the initial quiescent plateau (RP). (E) particles with top 10% value of the averaged local bond order parameter $\bar{q}_6$ in the configuration from which all trajectories were started (MRCO). (F) superimposed crystalline particles at $X = 0.1$ of 15 trajectories starting from different configurations. To better observe the density distribution, the particles' size has been reduced to 30% of their original size.

the main text, we identify avalanches by pinpointing the particles that displace beyond a certain threshold during a time interval of activity that separates two long quiescent plateaux in the mean squared displacement. An example of such time interval is shown by the red box in Fig. 6. Careful inspection of the avalanche shown in Fig. 6 reveals that it develops as a cascade of successive mini-avalanches separated by short-lived plateaux. This feature is shared by most avalanches we observe. We therefore define avalanche initiating particles (AIP) as those that move beyond $\sigma/3$ in a time interval that comprises *only the first* mini-avalanche (black box in Fig. 6). By superimposing the AIP of 20 trajectories starting from the same configuration – in fact, the configuration of Fig. 1 of the main text – with different sets of momenta we find that the propensity for an avalanche to be *initiated* (as opposed to avalanche *participation*) is clearly heterogeneously distributed (light-green dashed line in Fig. 5 (b) of the main text). Fig. 7, where the AIP propensity curves of two different halves of the total available trajectories are compared, shows that this result is statistically significant. Therefore, avalanches, like DH, tend to be triggered preferentially in particular regions of the system.

To investigate further any connection between avalanches and DH, we next inspect

Property	DH	A
Heterogeneous in space	Yes [14, 15]	Yes
Cooperative dynamics	Yes [16]	Yes
Stochastic in space and time	Yes [9, 17]	Yes
Spacial propensity	Yes [9]	Yes (initiation)
Propensity correlated to soft spots	Yes [10]	Further investigation required

TABLE I: Comparison between the properties of dynamic heterogeneities (DH) in supercooled fluids and avalanches (A) in a crystalizing hard sphere glass (this work).

whether AIP-rich regions are also rich in particles that have a high rattling freedom in the initial quiescent plateau. (Such rattlers are in turn equivalent to soft spots, which were found to be correlated to DH in metastable fluids [10–13]). In Fig. 8 we show the density profile of AIP particles compared to that of rattling particles (RP) for two set of simulations started from two different configurations. Our results are not conclusive, but offer plausible evidence of some correlation in at least one of these two configurations. If this is confirmed by future work, avalanches could plausibly be viewed as a limiting type of DH that arises when activity becomes rare as the system's density/age increases. In table I we summarize the comparison between the characteristics of avalanches in a crystallizing hard sphere glass and those of dynamic heterogeneities in a supercooled fluid.

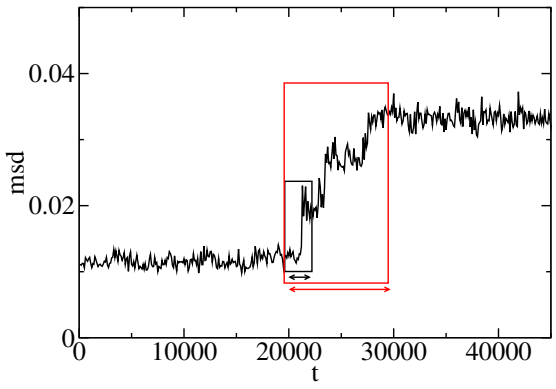

FIG. 6: Mean squared displacement versus time for one trajectory. The avalanche is indicated with a red square and the time interval in which the avalanche is defined is given by the red arrow. Whereas the avalanche initiation is indicated with a black square and the avalanche initiation period is given by the black arrow.

V. ONLINE VIDEO

The video (Movie SI) represents solid and avalanche particles participating to the avalanche shown in Fig. 1(b) of the main text. Solid-like particles are turquoise spheres and avalanche particles in $[t, (t + 1000t_0)]$ are red arrows with yellow heads. The avalanche starts to build in localized regions, then grows to peak activity, and finally dies out leaving behind an increased population of solid-like particles. Highly cooperative movements can be seen during the main avalanche phase, including particles moving in rows or circles. From

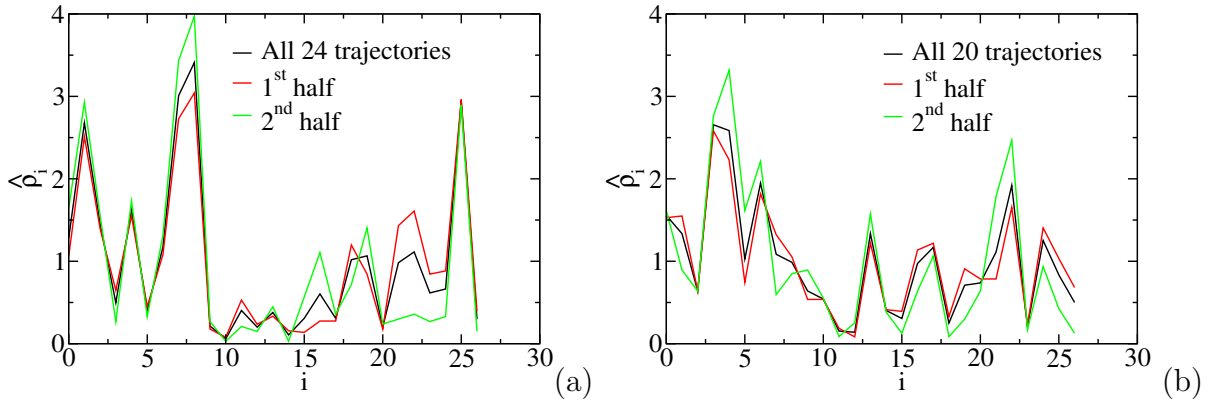

FIG. 7: Propensity curves of AIP using all available trajectories (black) and two different halves of them (red and green) to perform the analysis. Plots (a) and (b) correspond to two different starting configurations. Note that plot (a) corresponds to the same configuration as that analysed in Fig. 1 of the main text.

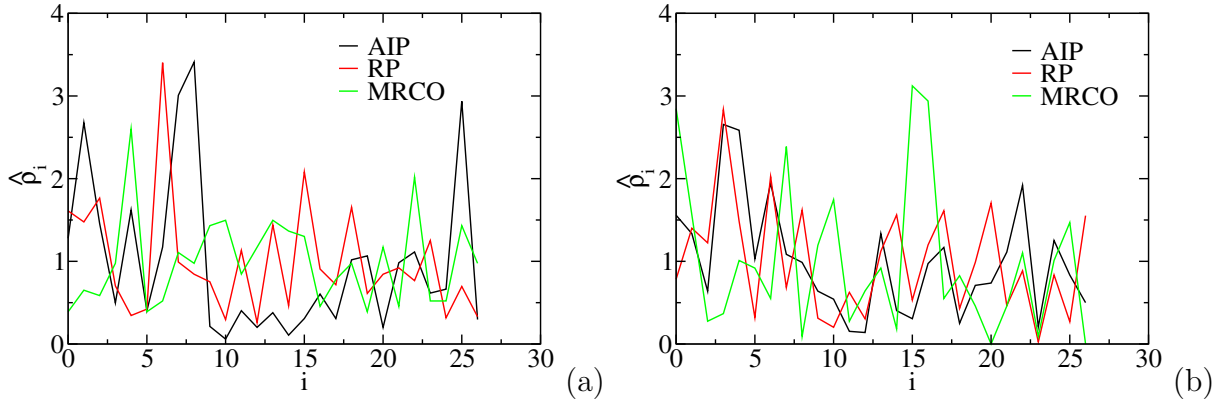

FIG. 8: Normalised density for the 27 sub-volumes in which the system is divided for different types of particles (as indicated in the legend) and for two different configurations (a) and (b). Plot (a) corresponds to the same configuration as that analysed in Fig. 1 of the main text.

start to finish, an avalanche typically lasts about $7000t_0$, with t_0 the time unit defined in the Methods Section.

[1] Sanz, E., Valeriani, C., Zaccarelli, E., Poon, W.C.K., Pusey, P.N. & Cates, M.E. Crystallization mechanism of hard sphere glasses. *Phys. Rev. Lett.* **106**, 215701 (2011).

[2] Alarcon L.M., Freccero M.A., Montani R.A.& Appignanesi, G.A. Determining the heterogeneity in time of the dynamics within a slowly relaxing region of a supercooled liquid: role of sharp relaxation events. *Phys. Rev. E* **80**, 026127 (2009).

[3] Stauffer, D. & Aharony, A. Introduction to percolation theory. *CRC Press* (1994).

[4] Valeriani, C., Sanz, E., Pusey, P.N., Poon, W.C.K., Cates, M.E. & Zaccarelli E. From compact to fractal crystalline clusters in concentrated systems of monodisperse hard spheres. *Soft Matter* **8**, 4960–4970 (2012).

[5] Valeriani, C., Sanz, E., Zaccarelli, E., Poon, W.C.K., Cates, M.E. & Pusey, P.N. Crystallization and aging in hard-sphere glasses. *J. Phys.:Condens. Matt.* **23**, 194117 (2011).

[6] Kawasaki, T., Araki, T., Tanaka, H. (2007) Correlation between dynamic heterogeneity and medium-range order in two-dimensional glass-forming liquids. *Phys. Rev. Lett.* 99:215701.

[7] Kawasaki, T. , Tanaka, H. (2010) Formation of a crystal nucleus from liquid. *Proc. Natl. Acad. Sci. USA* 107:14036–14041.

[8] Kawasaki, T. , Tanaka, H. (2010) Structural origin of dynamic heterogeneity in three-dimensional colloidal glass formers and its link to crystal nucleation. *J. Phys.: Condens. Matter* 22:232102.

[9] Widmer-Cooper, A., Harrowell, P. & Fynewever, H. How reproducible are dynamic heterogeneities in a supercooled liquid? *Phys. Rev. Lett.* **93**, 135701 (2004).

[10] Widmer-Cooper, A., Perry, H., Harrowell, P. , Reichman, D.R. (2008) Irreversible reorganization in a supercooled liquid originates from localized soft modes. *Nature Physics* 4:711–715.

[11] Brito, C., Wyart, M. (2009) Geometric interpretation of previtrification in hard sphere liquids. *J. Chem. Phys.* 131:024504.

[12] Widmer-Cooper, A., Perry, H., Harrowell, P., Reichman, D.R. (2009) Localized soft modes and the supercooled liquid's irreversible passage through its configuration space. *J. Chem. Phys.* 131:194508.

[13] Chen, K., Manning, M.L., Yunker, P.J., Ellenbroek, W.G., Zhang, Z., Liu, A.J., Yodh, A.G. (2011) Measurement of correlations between low-frequency vibrational modes and particle rearrangements in quasi-two-dimensional colloidal glasses. *Phys. Rev. Lett.* 107:108301.

[14] Schmidt-Rohr, K. and Spiess, H. W. (1991) Nature of Nonexponential Loss of Correlation above the Glass Transition Investigated by Multidimensional NMR *Phys. Rev. Lett.* 66:3020.

[15] Kob, W., Donati, C., Plimpton, S. J., Poole, P. H., Glotzer, S. C. (1997) Dynamical heterogeneities in a supercooled Lennard-Jones liquid. *Phys. Rev. Lett.* 79:2827.

[16] Donati, C., Douglas, J. F., Kob, W., Plimpton, S. J., Poole, P. H. and Glotzer, S. C. (1998) Stringlike Cooperative Motion in a Supercooled Liquid *Phys. Rev. Lett.* 80:2338.

[17] Appignanesi, G. A., Rodriguez Fris, J. A., Montani, R. A. and Kob, W. (2006) Democratic Particle Motion for Metabasin Transitions in Simple Glass Formers *Phys. Rev. Lett.* 96:057801.

Supporting Information

Sanz et al. 10.1073/pnas.1308338110

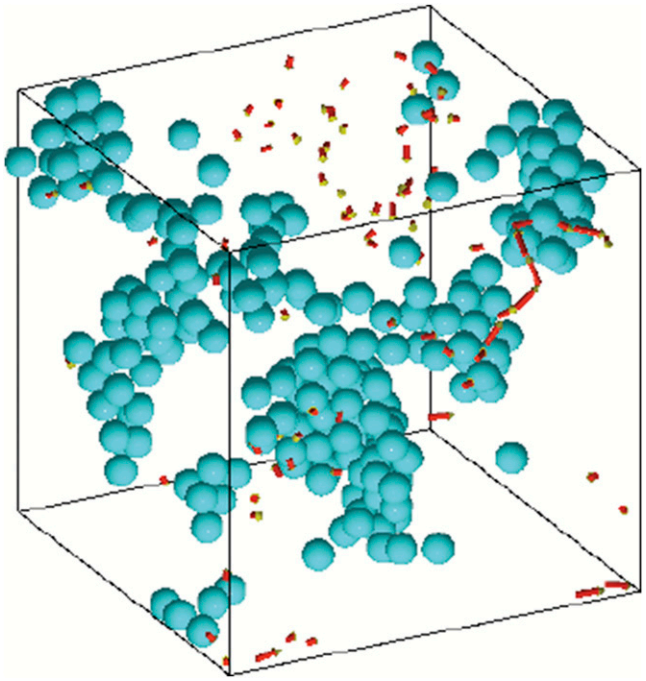

Movie S1. The movie represents solid and avalanche particles participating to the avalanche shown in Fig. 1*B* of the main text. The solid-like particles are turquoise spheres, and avalanche particles in $[t, (t + 1{,}000t_0)]$ are red arrows with yellow heads. The avalanche starts to build in localized regions, then grows to peak activity, and finally dies out, leaving behind an increased population of solid-like particles. Highly cooperative movements can be seen during the main avalanche phase, including particles moving in rows or circles. From start to finish, an avalanche typically lasts about $7{,}000t_0$, with t_0 the time unit defined in *Materials and Methods*.

Movie S1

Other Supporting Information Files

SI Appendix (PDF)